

UC Berkeley

UC Berkeley Previously Published Works

Title

Photocatalytic Stability of Single- and Few-Layer MoS₂

Permalink

<https://escholarship.org/uc/item/5hz2h8kr>

Journal

ACS Nano, 9(11)

ISSN

1936-0851

Authors

Parzinger, Eric
Miller, Bastian
Blaschke, Benno
[et al.](#)

Publication Date

2015-11-24

DOI

10.1021/acsnano.5b04979

Peer reviewed

This document is confidential and is proprietary to the American Chemical Society and its authors. Do not copy or disclose without written permission. If you have received this item in error, notify the sender and delete all copies.

Photocatalytic Stability of Single- and Few-Layer MoS₂

Journal:	ACS Nano
Manuscript ID	nn-2015-04979t.R1
Manuscript Type:	Article
Date Submitted by the Author:	n/a
Complete List of Authors:	Parzinger, Eric; Technische Universität München, Walter Schottky Institut and Physik-Department; Nanosystems Initiative Munich (NIM), Miller, Bastian; Technische Universität München, Walter Schottky Institut and Physik-Department; Nanosystems Initiative Munich (NIM), Blaschke, Benno; Technische Universität München, Walter Schottky Institut and Physik-Department Garrido, Jose; Technische Universität München, Walter Schottky Institut and Physik-Department Ager, Joel; Lawrence Berkeley National Laboratory, Joint Center for Artificial Photosynthesis Holleitner, Alexander; Technische Universität München, Walter Schottky Institut and Physik-Department; Nanosystems Initiative Munich (NIM), Wurstbauer, Ursula; Technische Universität München, Walter Schottky Institut and Physik-Department; Nanosystems Initiative Munich (NIM),

SCHOLARONE™
Manuscripts

Photocatalytic Stability of Single- and Few-Layer MoS₂

Eric Parzinger^{,†,‡}, Bastian Miller^{†,‡}, Benno Blaschke[†], Jose A. Garrido[†], Joel W. Ager[‡],
Alexander Holleitner^{†,‡} and Ursula Wurstbauer^{*,†,‡}*

[†]Walter Schottky Institut and Physik-Department, Technische Universität München, Am
Coulombwall 4a, 85748 Garching, Germany

[‡]Nanosystems Initiative Munich (NIM), Munich 80799, Germany

[‡]Joint Center for Artificial Photosynthesis, Lawrence Berkeley National Laboratory, Berkeley,
California 94720, USA

*Address correspondence to eric.parzinger@wsi.tum.de or wurstbauer@wsi.tum.de.

Keywords: Two-dimensional materials, MoS₂, Photocatalytic stability, Photocatalytic selectivity, solar water splitting, Raman spectroscopy

ABSTRACT

MoS₂ crystals exhibit excellent catalytic properties and great potential for photo-catalytic production of solar fuel such as hydrogen gas. In this regard, the photocatalytic stability of exfoliated single- and few-layer MoS₂ immersed in water is investigated by μ -Raman spectroscopy. We find that while the basal plane of MoS₂ can be treated as stable under

1
2
3 photocatalytic conditions, the edge sites and presumably also defect sites are highly affected by a
4 photo-induced corrosion process. The edge sites of MoS₂ monolayers are significantly more
5 resistant to photocatalytic degradation compared to MoS₂ multi-layer edge sites. The photo-
6 stability of MoS₂ edge sites depends on the photon energy with respect to the band gap in MoS₂
7 and also on the presence of oxygen in the electrolyte. These findings are in agreement with an
8 interpretation as oxidation process converting MoS₂ into MoO_x in the presence of oxygen and
9 photo-induced charge carriers. The high stability of the MoS₂ basal plane under photocatalytic
10 treatment with visible light irradiation of extreme light intensities in the order of $P \approx 10\text{mW}/\mu\text{m}^2$
11 substantiates MoS₂'s potential as photocatalyst for solar hydrogen production.
12
13
14
15
16
17
18
19
20
21
22
23
24
25

26 MoS₂ is a semiconducting two-dimensional 'van der Waals' material with outstanding
27 electronic,^{1,2} optical³⁻⁵ and catalytic⁶⁻⁸ properties. MoS₂ undergoes a transition from an indirect
28 to a direct band gap semiconductor in the single layer limit³ with a band gap of $E_{\text{gap}} = 1.9\text{ eV}$.⁴
29 The high sunlight absorption of up to 10% for atomistic thin layers⁹ makes MoS₂ single- but also
30 few-layers a promising material for optoelectronic applications and solar energy harvesting. For
31 pH values between 0 and 7, a single layer of MoS₂ exhibits a suitable band edge alignment with
32 respect to the redox potentials of the hydrogen evolution (H⁺/H₂) (HER) and oxygen evolution
33 (O₂/H₂O) (OER) reaction,^{10,11} which is an unambiguous requirement of a photo-catalyst for solar
34 driven water splitting with an earth abundant electrolyte such as river or sea water. The
35 peculiarity of MoS₂ is that it holds all requirements for a monolithic device for solar water
36 splitting, because MoS₂ based materials offer not only catalytic activity,⁶⁻⁸ but also high
37 absorption efficiency in the visible range.⁹ The basal planes feature the functionalization as photo
38 absorber, built-in electric fields induced *e.g.* by lateral pn-junctions separate the e-h pairs¹² and
39 the Mo edge along (10 $\bar{1}$ 0) direction is catalytically active.¹³ If a photon is absorbed by an
40
41
42
43
44
45
46
47
48
49
50
51
52
53
54
55
56
57
58
59
60

1
2
3 interband absorption process, the incoming photon promotes an electron from the valence band
4
5 to the conduction band leaving a hole in the valence band. Such photoexcited electrons can be
6
7 directly transferred from the conduction band to the energetically preferred potential of the
8
9 proton reduction. The transferred electron drives the hydrogen evolution reaction. The same
10
11 applies for the photoexcited holes and the oxygen evolution reaction. Thus, single-layer MoS₂
12
13 serves as an ideal candidate for an efficient photocatalyst powering the sunlight-driven
14
15 photocatalytic water splitting reaction.
16
17
18
19

20
21 Considerable efforts have been made to investigate the catalytic activity of various MoS₂
22
23 nanostructures such as nanoparticles,^{6,14,15} mesopores,¹⁶ nanowires,¹⁷ amorphous MoS₂,^{18–20} thin
24
25 films²¹ and their nanostructure,¹³ MoS₂/graphene heterostructures,²² chemically exfoliated MoS₂
26
27 layers,^{7,23,24} metal nanoparticle-decorated MoS₂²⁵ and MoS₂ grown by chemical vapor
28
29 deposition.⁸ Nonetheless, the long term photo-catalytical stability, and not only catalytical
30
31 stability, is a crucial but often ignored requirement for photo-absorber and catalytic materials in
32
33 water splitting devices.²⁶ For electro-catalysts, potential cycling with different scan rates and
34
35 potential ranges in the dark are the most common methods to address the catalytic stability.^{21,22,27}
36
37 For photocatalytically active materials, however, the catalytic stability in the presence of light
38
39 irradiation is essential since catalytically stable materials are not per se stable under light
40
41 irradiation. MoS₂ has been integrated in a silicon tandem photo-electrochemical water splitting
42
43 device acting as electro-catalyst and simultaneously as corrosion protection for the Si photo-
44
45 absorber.^{28,29} Stability in HER conditions measured by cyclic voltammetry under 1 sun red
46
47 irradiation (E_L < 1.95 eV) has been demonstrated.²⁸ Bulk and nanostructured MoS₂ materials are
48
49 efficient and stable photo-cathodes showing sun-light driven HER in a monolithic metal-free
50
51
52
53
54
55
56
57
58
59
60

1
2
3 architecture, however progressive photocorrosion under OER conditions limits its
4
5 functionalization as photoanode because of anodic photo-corrosion along the $\langle 11\bar{2}0 \rangle$ direction.¹³
6
7

8
9 In this letter, we introduce μ -Raman spectroscopy in aqueous environment to microscopically
10 investigate the stability of well-defined high-quality single- and few-layer MoS₂ crystals under
11 photocatalytic conditions. Of particular interest is the role of the number of layers and hence the
12 impact of the nature of the band gap as well as the role of exciton effects on the stability of the
13 basal plane and edge sites in an earth abundant electrolyte - fresh water. The measurement
14 scheme applies a monochromatic irradiation with high light intensities of $P \approx 10 \text{ mW}/\mu\text{m}^2$ what
15 would be equivalent to 10^7 suns. Photostability under such challenging conditions certifies a
16 material as durable and can be treated as long-term stable. Long-term stability of MoS₂ in
17 aqueous solutions and in high humidity is not only important for solar-driven water splitting, but
18 also for sensing applications, for functional corrosion protection layer and in general for
19 electronic applications.
20
21
22
23
24
25
26
27
28
29
30
31
32
33
34
35

36 Thus, the photo-degradation of MoS₂ flakes immersed in water is *in situ* monitored with a high
37 lateral resolution of about 300 nm and a time resolution of a few seconds. The photo-stability
38 and the evolution of photo-degradation of MoS₂ in presence of water as electrolyte is studied in
39 dependence of crystallographic site, number of layers, energy and intensity of the exposing light
40 as well as the presence of oxygen gas in the electrolyte. We find that the more catalytically active
41 edge sites³⁰⁻³³ show a much higher photo-degradation compared to the basal plane (a.k.a. terrace
42 sites). We further observe that edge sites of MoS₂ monolayers exhibit a much lower degradation
43 rate compared to edge sites of few-layers with corresponding decay rates of $\tau = 45 \text{ min}$ and $\tau = 1$
44 min for mono- and bilayer, respectively. Photo-degradation for flakes immersed in water takes
45 place only under irradiation with energy larger than the band-gap of MoS₂. In addition, in our
46
47
48
49
50
51
52
53
54
55
56
57
58
59
60

1
2
3 experiments the presence of oxygen in the electrolyte is required to observe a considerable
4
5 photo-degradation of the flakes edge sites. Overall, MoS₂ basal planes exhibit superior photo-
6
7 stability in aqueous environment under extreme irradiation intensities und even the catalytically
8
9 active edge site are rather stable in the absence of O₂ in the electrolyte.
10
11

12 13 14 RESULTS AND DISCUSSION

15
16
17 The investigated MoS₂ flakes are micromechanically exfoliated from bulk crystals and
18
19 transferred to Si/SiO₂ substrates by a dry stamping technique.³⁴ The SiO₂ thickness of 275 nm
20
21 provide an excellent visibility contrast^{35,36} so that even single layers of MoS₂ are clearly
22
23 distinguishable from bi-, tri- and few-layer regions by optical microscopy as well as by
24
25 monochromatic reflectivity measurements. The samples are characterized prior and after the
26
27 photocatalytic degradation studies by a set of microscopy and spectroscopy tools under ambient
28
29 conditions. Size and changes in geometry are investigated by contrast images from optical
30
31 microscopy, and monochromatic reflectivity measurements by scanning a laser with low power
32
33 and high sampling rate over the sample and recording the reflected light with a photo-diode. The
34
35 morphology is investigated by atomic force microscopy. From spatially resolved Raman
36
37 spectroscopy, we gain access to various parameters such as the number of layers,³⁷ doping level³⁸
38
39 and even the presence of adsorbates.³⁹ Furthermore, the degradation process is monitored *in situ*
40
41 by real-time Raman spectroscopy utilizing the irradiation laser of the photo-degradation studies
42
43 for the Raman measurements. The most important figure of merits in the presented experiments
44
45 is the time evolution of the phonon-mode energies as fingerprint for the number of layers and the
46
47 change in the integrated intensity of the individual modes as sensor for the amount of unaffected
48
49 and not photo-degraded crystalline volume. A high spatial resolution for all optical
50
51 measurements in liquid is realized through a laser spot size of about 300 nm given by a water-
52
53
54
55
56
57
58
59
60

1
2
3 dipping objective and mounting the sample on x - y - z piezo scanner. If not stated otherwise,
4
5 deionized (DI) water is used as electrolyte.
6
7

8
9 Figure 1 demonstrates the photo-stability of a mono-/trilayer flake under irradiation with a
10 focused laser with energy $E_{laser} = 2.54$ eV. This energy is larger than the band-gap of MoS₂ (E_{gap}
11 = 1.9eV). The region of interest (ROI) is marked on the optical microscopy image in Figure 1(a).
12
13 The laser is scanned across a field consisting of monolayer (1L) and trilayer (3L) parts along the
14 path shown on the reflectivity image in Figure 1(b) (on the right). The laser with a power of P_{laser}
15 = 1 mW is kept at each spot for 20 s, and the step size during the scanning process is 250 nm.
16
17 The sample is completely immersed in DI water during the whole scan. Figure 1(b) shows the
18 reflectivity image taken prior (left side) and after exposure to laser light (right side). The right
19 side discloses that the whole scanned 3L region is thinned down, whereas part of the 1L region
20 seems to be unaffected. Other parts of the monolayer region are missing. In a next step, Raman
21 measurements in ambient conditions are recorded on several positions on the MoS₂ flake [Figure
22 1(c)]: untreated 3L region (◆), thinned 3L region (▲), affected 1L (●) and untreated 1L region
23 (■). The two characteristic zone-center phonons of MoS₂ are observable in the spectra. The E_{2g}^1
24 mode is an in-plane mode, with the atoms oscillating parallel to the basal plane and the A_{1g} mode
25 is an out-of-plane oscillation with the sulfur atoms oscillating in opposite direction as sketched in
26 Figure 2. The Raman measurements confirm the observation already seen from the reflectivity
27 measurements. The Raman spectrum within the thinned area (▲) matches that of a monolayer,
28 except a slight shift of the A_{1g} mode towards higher wavenumbers. This upshift in energy of ~ 0.3
29 cm^{-1} can be explained by a decreased charge carrier density, consistent with an increased number
30 of adsorbed molecules on defect sites.^{39–41} The reminiscent weak Raman intensities at the
31 degraded monolayer region (●) is either attributed to a diluted amount of residual MoS₂
32
33
34
35
36
37
38
39
40
41
42
43
44
45
46
47
48
49
50
51
52
53
54
55
56
57
58
59
60

1
2
3 nanoflakes or to the fact that the spatial resolution of the water dipping objective is decreased by
4
5 the measurements without liquid. The Raman spectra further demonstrate that the non-exposed
6
7
8 3L (◆) and 1L areas (■) are unaffected and consequently stable in water without illumination.
9

10
11 To study the photo-corrosion process in more detail, we repeatedly record Raman spectra on a
12
13 different sample with bi-layer MoS₂ edges as well as basal planes. Again, the excitation energy is
14
15 chosen to be above the band gap ($E_{laser} = 2.54$ eV). The measurements are carried out for various
16
17 light intensities on various spots containing edge or terrace sites exemplarily demonstrated on the
18
19 flake shown in Figure 2(a). The temporal evolution of energy as well as intensity of the two
20
21 relevant phonon modes A_{1g} and E¹_{2g}, whose oscillation schemes are sketched in Figure 2(b),
22
23 enable us to *in situ* monitor the photo-induced degradation process with a high spatial resolution
24
25 by Raman scattering. Figures 2(c) and (d) depict the temporal evolution of the integrated
26
27 intensities of the phonon modes recorded on the edge sites marked in Figure 2(a) for different
28
29 light intensities. For clarity and better comparability, the peaks are normalized to their initial
30
31 intensity. The related Raman spectra are plotted in Figure 2(e) for $t = 0$ sec (◆) and in Figure 2(f)
32
33 after $t \approx 1$ min (○). At the beginning of the measurement ($t = 0$ sec) marked by (◆) in Figures
34
35 2(c,d), the energies of the relevant phonon modes are unambiguously corresponding to those of
36
37 bi-layer MoS₂ [Figure 2(e)]. After approximately 1 minute, marked by (○) in panels (c,d), the
38
39 signal of both Raman modes drop to about 50% of the initial intensities. Simultaneously, the E¹_{2g}
40
41 Raman mode is blue-shifted and the A_{1g} Raman mode is redshifted. This change in the photon
42
43 energies definitely marks the transition from a MoS₂ bi-layer to a MoS₂ monolayer³⁷ after ~1
44
45 min of light exposure [Figure 2(f)]. The photo-induced transition from bi- to monolayer MoS₂ is
46
47 in line with the fact that the recorded Raman signals of both phonon modes disclose two distinct
48
49 degradation rates. These rates exhibit an exponential decay rate of $\tau \approx 1$ min and $\tau \approx 45$ min,
50
51
52
53
54
55
56
57
58
59
60

1
2
3 respectively. Therefore, the initial fast decay rate can be interpreted as the stability of the bi-layer
4
5 edge site, whereas the much slower decay rate is the stability of the monolayer. For comparison,
6
7 Figure 2(g) depicts the temporal evolution of the normalized integrated intensity of the silicon
8
9 TO-phonon mode. The intensity of the Si-phonon mode increases by a similar amount as the
10
11 intensity of the two MoS₂-phonon modes decreases approaching the intensity value of the Si-
12
13 mode on the pristine substrate. This opposite trend of the intensities of Si and MoS₂ phonon
14
15 modes, respectively, corroborates the above given interpretation that the drop in intensity of the
16
17 Raman modes of the photo-excited MoS₂ is because of photo-degradation of the material and
18
19 that it is not caused by spurious effects like the loss of laser focus. The overall exponential decay
20
21 is power independent between 0.5 mW and 1.5 mW [Figures 2(c) and (d)]. This is interpreted
22
23 such that the corrosion process is already saturated with a laser power of 0.5 mW. The photo-
24
25 degradation is most likely limited by a rather slow oxidation rate linked to the density of mobile
26
27 holes η_{th} in MoS₂, but not directly linked to the absolute density of photo-excited charge carriers
28
29 η and the oxidation rate is presumably also affected by the diffusion of reactive species present
30
31 in the electrolyte. The rate is expected to be slower than the turn over frequency (TOF) for the
32
33 HER reported to be TOF = 0.02 s⁻¹ per MoS₂ edge site.³⁰ The density of photo-induced e-h pairs
34
35 constitutes approximately $\eta > 10^{11}$ cm⁻² for a spot diameter of ~300 nm, laser wavelength of 488
36
37 nm, an absorption efficiency of ~ 10% and an e-h recombination slower than 1 ps.⁴² The number
38
39 of freely mobile holes η_{th} is expected to be larger for the bilayer because of the combined effect
40
41 of a reduced exciton binding energy from 0.64 eV⁴³ for the monolayer to less than 0.21 eV
42
43 (number for MoSe₂, similar value expected for MoS₂)⁴⁴ for bilayers and by an increased lifetime
44
45 of the holes as expected for an indirect bandgap semiconductors.
46
47
48
49
50
51
52
53
54
55
56
57
58
59
60

1
2
3 We now reveal the role of number of layers as well as the difference between edge and terrace
4 sites for the photo-corrosion process. We illuminate several MoS₂ samples consisting of mono-
5
6 and few-layer regions with three different geometries: either scanning the laser across a field on
7
8 the sample in a specific pattern as shown *e.g.* in Figure 1, illuminating a spot either on the
9
10 samples' edge or basal plane (see Figure 2) or scanning the laser along a line from the substrate
11
12 onto the flake across steps from mono- to multilayer region or *vice versa* and back from the flake
13
14 to the substrate as demonstrated on the MoS₂ flake in Figure 3.
15
16
17
18
19

20
21 Figure 3 depicts an optical micrograph and an atomic force microscopy (AFM) image with
22
23 corresponding height profile before and after a laser line scan from the substrate across a trilayer
24
25 to a protruding monolayer area. The transition from substrate over the edge of the trilayer region
26
27 is marked as (1), the transition from trilayer to the protruding monolayer with (2) and over the
28
29 monolayer edge site to the substrate with (3). The laser scan is performed with the sample
30
31 immersed in DI water, a laser excitation energy of 2.54 eV (488 nm), a step size of 100 nm and a
32
33 dose of 200 μW x 120 s at each spot. The removal of the trilayer part starting at the edge site (1)
34
35 is clearly visible, while the single layer seems almost unaffected as evident in the AFM height
36
37 profiles perpendicular to the line of the laser scan. The monolayer seems to be undamaged at
38
39 transition (2) from tri- to monolayer without hitting a monolayer edge and is visibly only
40
41 affected at the step (3) from the monolayer region to the substrate. This linescan shows that the
42
43 edge sites are degraded after illumination in water, whereas the basal plane remains visibly
44
45 unaffected in agreement with the previous reported findings.
46
47
48
49
50
51

52
53 Focusing the laser on a single spot on the basal plane of a trilayer yields no corrosion of the
54
55 flake on a similar timescale and irradiation dose. Such a difference in the photo-degradation
56
57 between edge and basal plane has been observed for all investigated flakes. The terrace site can
58
59
60

1
2
3 be treated as stable under the assumption that the photo-corrosion observed *e.g.* in Figure 1 on
4 the 1L part starts on defect sites. Like edge sites, defect sites imply dangling bonds that are
5
6 the 1L part starts on defect sites. Like edge sites, defect sites imply dangling bonds that are
7
8 expected to be responsible for the enlarged catalytic activity compared to the basal plane. The
9
10 absence of dangling bonds at the basal planes is characteristic for van-der Waals layered
11
12 materials such as MoS₂.
13
14

15
16 We find that the photo-excitation of electron-hole pairs is essential for the photo-degradation
17
18 process. The MoS₂ edge sites only degrade under light exposure with energies larger than the
19
20 band gap. Figure 4 contrasts two optical images of the same flake after laser scans conducted
21
22 with an energy of $E_{laser} = 1.59$ eV and $E_{laser} = 2.54$ eV, corresponding to illumination with energy
23
24 smaller and larger than the direct band gap of MoS₂, respectively. For the lower irradiation
25
26 energy, no corrosion shows up neither on the MoS₂ edge nor on the illuminated basal planes
27
28 (laser power $P_{laser} = 1.5$ W). The complementary scan with light energy of 2.54 eV ($P_{laser} = 0.5$
29
30 W), however, clearly displays a decomposition of the flake over a large area. From the scan
31
32 direction of the laser, marked by the arrows in Figure 4, we again see that the photo-degradation
33
34 predominantly starts at the step-edges of the individual planes.
35
36
37
38
39

40
41 Let us now turn to the role of reactive species in the electrolyte. The power-independence of
42
43 the photo-degradation rate [Figure 2(e) and (f)] points already towards the importance of reactive
44
45 species and their amount on the interface between MoS₂ and electrolyte. Their role is
46
47 investigated on example of oxygen as reactive species by changing the amount of dissolved
48
49 oxygen in the DI water. To this end, the photo-stability of edge sites of a bi-layer flake immersed
50
51 in degassed DI water is studied with parameters similar to those shown in Figure 2. The DI water
52
53 is degassed with inert nitrogen gas in order to reduce the amount of naturally dissolved oxygen.
54
55
56 The photo-degradation rates of MoS₂ bilayers immersed in water with and without oxygen are
57
58
59
60

1
2
3 compared in Figure 5. The drop in the MoS₂ Raman intensities monitoring the degradation is
4 indeed significantly reduced, when the sample is immersed in water with a strongly reduced
5 oxygen concentration. The remaining degradation rate might be influenced by the steadily
6 increasing oxygen content in the DI water over time. During the measurements, the surface of
7 the water basin is in contact to ambient air and consequently it is expected that the nitrogen gas
8 dissolved in the electrolyte is again replaced by oxygen gas.
9

10
11 Overall, all our observations are in agreement with the interpretation that MoS₂ terrace sites
12 immersed in water as electrolyte can be treated as stable under photocatalytic conditions even
13 under extreme irradiation intensity of 10 mW/μm². Edges and presumably also defects sites,
14 however, exhibit a significant, photo-generated charge carrier driven catalytic degradation in the
15 presence of reactive species such as oxygen. Opposite to reported laser thinning, where thermal
16 ablation caused by laser heating is used to thin MoS₂ to monolayers,⁴⁵ the process reported here
17 is of significant different origin. Thermal ablation causes are unlikely to produce the observed
18 photodegradation because of the low laser power, absence of a power dependence, the distinct
19 difference between edge sites and basal plane and also the absence of degradation for light
20 energy below the band gap. We propose a charge carrier driven photo-catalytic oxidation process
21 converting MoS₂ into MoO₃ or more general into MoO_x as the underlying process for the photo-
22 degradation. The MoO_x then dissolves in the electrolyte⁸ in agreement with the absence of any
23 MoO_x signatures in a suitable energy range in Raman spectroscopy. This photo-corrosion
24 process is believed to be responsible for the photo-degradation of MoS₂ at area-scans, line-scans
25 as well as spot-like exposure of edge sites with light above the band-gap. The amount of
26 dissolved MoO_x in the electrolyte from a 1 μm x 1 μm oxidized area of a flake would result in
27 approximately 10⁻¹⁴ g of MoO_x in more than 1 ml water in a petri dish that is not sealed against
28
29
30
31
32
33
34
35
36
37
38
39
40
41
42
43
44
45
46
47
48
49
50
51
52
53
54
55
56
57
58
59
60

1
2
3 the environment. For this reason it is not possible in this study to further investigate the MoO_x
4
5 compound *e.g.* by inductively coupled plasma mass spectrometry.
6
7

8
9 The fact that we observe photo-corrosion predominantly on edge sites can be explained by a
10
11 more favored transfer of charge carriers to the electrolyte from edge and defect sites due to
12
13 existent dangling bonds compared to the basal plane without dangling bonds. The found
14
15 degradation on some individual spots on the basal plane suggest to start at lattice defects. Such
16
17 individual defects of the crystal are beyond the resolution in our experiments and therefore we
18
19 can only conjecture about the role of defect sites. The observed layer dependence is interpreted
20
21 in terms of an increased density of freely mobile holes η_{fh} for MoS₂ bi- and multilayers
22
23 compared to the monolayer because of a much larger exciton-binding energy for the monolayer
24
25 resulting in a reduced e-h separation efficiency. The observed layer dependence might be further
26
27 amplified by an increased life-time of photo-generated charge carriers due to the reduced
28
29 recombination rate for the indirect band-gap of MoS₂ bi-, tri- and multilayers compared to the
30
31 direct band gap in the monolayer limit. A role of the supporting substrate is unlikely since we
32
33 assume a thin water layer between the MoS₂ flake and the hydrophilic SiO₂ substrates as the
34
35 exfoliation process has not been done in inert atmosphere. This assumption is supported by
36
37 atomic force microscopy height profile revealing a step height from substrate to MoS₂ monolayer
38
39 of about 3 nm, whereas the step height from monolayer to bilayer constitutes 0.7 nm close to the
40
41 theoretical value.
42
43
44
45
46
47
48

49 50 **CONCLUSION**

51
52
53 In summary, we find that the MoS₂ edge sites are subject to significant photo-corrosion under
54
55 light exposure with a laser energy larger than the direct band gap, when immersed in an
56
57
58
59
60

1
2
3 electrolyte with dissolved oxygen. The photo-corrosion process is found to take place on edge
4
5 and most likely also defect sites. The photo-degradation rate is much faster for bi- and multi-
6
7 layer ($\tau_1 \sim 1$ min) compared to monolayer ($\tau_2 \sim 45$ min) MoS₂ and is explained by the transition
8
9 from an indirect to a direct semiconductor resulting in an decreased amount of freely mobile
10
11 photogenerated holes η_{th} due to an increased exciton binding energy and reduced lifetime of the
12
13 charge carriers. The degradation process is interpreted in terms of an oxidation process driven by
14
15 the photo-generated charge carriers converting MoS₂ *e.g.* into MoO_x that is expected to be
16
17 dissolved in the electrolyte. The role of photo-generated charge carriers as driving force can
18
19 explain the layer-dependence as well as the superior catalytic degradation of the edges compared
20
21 to basal planes.
22
23
24
25
26
27

28 The MoS₂ basal plane is found to exhibit a high level of photocatalytic stability even in the
29
30 presence of reactive species such as oxygen in the electrolyte and under irradiation with visible
31
32 light of intensities exceeding 10 mW/ μm^2 . The stability in photocatalytic conditions is an
33
34 unambiguous requirement of a photo-absorber for photocatalytic splitting of water, but also for
35
36 sensing applications, transparent corrosion protection layer with further functionality and general
37
38 for optoelectronic device applications in aqueous or humid environment. The stability under
39
40 challenging conditions together with high absorption in the visible range and the electro-catalytic
41
42 activity strengthen MoS₂'s potential for sunlight driven overall hydrogen production by water
43
44 splitting in a durable monolithic device without any metals utilizing the earth abundant
45
46 electrolyte fresh water.
47
48
49
50

51 52 53 **METHODS** 54 55 56 57 58 59 60

1
2
3 MoS₂ flakes are prepared by standard micromechanical exfoliation from bulk crystal (SPI
4 supplies) and then transferred to a p-type doped Si substrate with a 275 nm thick thermal oxide
5 layer on top. The transfer is accomplished by an all-dry viscoelastic stamping technique³⁴ using a
6 polydimethylsiloxane (PDMS) thin film. The flakes are investigated by optical contrast, scanning
7 reflectivity measurements, atomic force microscopy as well as Raman spectroscopy.
8
9

10
11
12
13
14
15
16 All optical measurements, reflectivity scans as well as μ -Raman spectroscopy and laser cutting
17 with the sample immersed in the electrolyte are performed using a 63x water immersion
18 objective (Carl Zeiss Objective W N-Achroplan 63x/0.9 M27) in combination with a piezo stack
19 with a closed-loop resolution of 1 nm (Physik Instrumente P-611.3 NanoCube[®] XYZ-System).
20
21 This combination allows us to reach a spatial resolution of roughly 300 nm in our measurements
22 with the sample in the electrolyte. The position of the flake is monitored before and after each
23 measurement in order to exclude any influence due to lateral drifts. Laser excitation energies
24 below ($\lambda = 780$ nm) and above the direct band gap energy ($\lambda = 488$ nm) are accessed utilizing a
25 Ti:Sapphire and Ar-ion gas laser, respectively, as excitation light source.
26
27
28
29
30
31
32
33
34
35
36
37

38 AUTHOR INFORMATION

39 Corresponding Author

40
41 *E-Mail: eric.parzinger@wsi.tum.de (E.P.).
42

43 *E-Mail: ursula.wurstbauer@wsi.tum.de (U.W).
44
45
46
47

48 Author Contributions

49
50 The manuscript was written through contributions of all authors. All authors have given approval
51 to the final version of the manuscript.
52
53
54

55 Funding Sources

56
57
58
59
60

1
2
3 We acknowledge financial support by the DFG *via* excellence cluster Nanosystems Initiative
4
5 Munich (NIM) and project Ho 3324/8-1 as well as BaCaTeC.
6
7

8 9 **ABBREVIATIONS**

10
11 HER, hydrogen evolution reaction; OER, oxygen evolution reaction; e-h, electron-hole; DI,
12
13 deionized; atomic force microscopy (AFM);
14
15

16 17 **REFERENCES**

- 18
19
20 1. Radisavljevic, B.; Radenovic, A.; Brivio, J.; Giacometti, V.; Kis, A. Single-Layer MoS₂
21
22 Transistors. *Nat. Nanotechnol.* **2011**, *6*, 147–150.
23
24
- 25
26 2. Wang, Q. H.; Kalantar-Zadeh, K.; Kis, A.; Coleman, J. N.; Strano, M. S. Electronics and
27
28 Optoelectronics of Two-Dimensional Transition Metal Dichalcogenides. *Nat.*
29
30 *Nanotechnol.* **2012**, *7*, 699–712.
31
32
- 33
34 3. Splendiani, A.; Sun, L.; Zhang, Y.; Li, T.; Kim, J.; Chim, C.-Y.; Galli, G.; Wang, F.
35
36 Emerging Photoluminescence in Monolayer MoS₂. *Nano Lett.* **2010**, *10*, 1271–1275.
37
38
- 39
40 4. Mak, K. F.; Lee, C.; Hone, J.; Shan, J.; Heinz, T. F. Atomically Thin MoS₂: A New
41
42 Direct-Gap Semiconductor. *Phys. Rev. Lett.* **2010**, *105*, 136805.
43
44
- 45
46 5. Mak, K. F.; He, K.; Shan, J.; Heinz, T. F. Control of Valley Polarization in Monolayer
47
48 MoS₂ by Optical Helicity. *Nat. Nanotechnol.* **2012**, *7*, 494–498.
49
- 50
51 6. Hinnemann, B.; Moses, P. G.; Bonde, J.; Jørgensen, K. P.; Nielsen, J. H.; Horch, S.;
52
53 Chorkendorff, I.; Nørskov, J. K. Biomimetic Hydrogen Evolution: MoS₂ Nanoparticles
54
55 as Catalyst for Hydrogen Evolution. *J. Am. Chem. Soc.* **2005**, *127*, 5308–5309.
56
57
58
59
60

- 1
2
3
4
5
6
7
8
9
10
11
12
13
14
15
16
17
18
19
20
21
22
23
24
25
26
27
28
29
30
31
32
33
34
35
36
37
38
39
40
41
42
43
44
45
46
47
48
49
50
51
52
53
54
55
56
57
58
59
60
7. Chhowalla, M.; Shin, H. S.; Eda, G.; Li, L.-J.; Loh, K. P.; Zhang, H. The Chemistry of Two-Dimensional Layered Transition Metal Dichalcogenide Nanosheets. *Nat. Chem.* **2013**, *5*, 263–275.
8. Yu, Y.; Huang, S.-Y.; Li, Y.; Steinmann, S. N.; Yang, W.; Cao, L. Layer-Dependent Electrocatalysis of MoS₂ for Hydrogen Evolution. *Nano Lett.* **2014**, *14*, 553–558.
9. Bernardi, M.; Palumbo, M.; Grossman, J. C. Extraordinary Sunlight Absorption and One Nanometer Thick Photovoltaics Using Two-Dimensional Monolayer Materials. *Nano Lett.* **2013**, *13*, 3664–3670.
10. Li, Y.; Li, Y.-L.; Araujo, C. M.; Luo, W.; Ahuja, R. Single-Layer MoS₂ as an Efficient Photocatalyst. *Catal. Sci. Technol.* **2013**, *3*, 2214–2220.
11. Zhuang, H. L.; Hennig, R. G. Computational Search for Single-Layer Transition-Metal Dichalcogenide Photocatalysts. *J. Phys. Chem. C* **2013**, *117*, 20440–20445.
12. Choi, M. S.; Qu, D.; Lee, D.; Liu, X.; Watanabe, K.; Taniguchi, T.; Yoo, W. J. Lateral MoS₂ P–n Junction Formed by Chemical Doping for Use in High-Performance Optoelectronics. *ACS Nano* **2014**, *8*, 9332–9340.
13. Chen, Z.; Forman, A. J.; Jaramillo, T. F. Bridging the Gap Between Bulk and Nanostructured Photoelectrodes: The Impact of Surface States on the Electrocatalytic and Photoelectrochemical Properties of MoS₂. *J. Phys. Chem. C* **2013**, *117*, 9713–9722.
14. Bonde, J.; Moses, P. G.; Jaramillo, T. F.; Nørskov, J. K.; Chorkendorff, I. Hydrogen Evolution on Nano-Particulate Transition Metal Sulfides. *Faraday Discuss.* **2008**, *140*, 219–231.

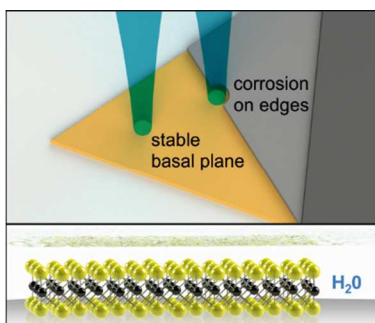
- 1
2
3
4
5
6
7
8
9
10
11
12
13
14
15
16
17
18
19
20
21
22
23
24
25
26
27
28
29
30
31
32
33
34
35
36
37
38
39
40
41
42
43
44
45
46
47
48
49
50
51
52
53
54
55
56
57
58
59
60
15. Vrubel, H.; Merki, D.; Hu, X. Hydrogen Evolution Catalyzed by MoS₃ and MoS₂ Particles. *Energy Environ. Sci.* **2012**, *5*, 6136–6144.
16. Kibsgaard, J.; Chen, Z.; Reinecke, B. N.; Jaramillo, T. F. Engineering the Surface Structure of MoS₂ to Preferentially Expose Active Edge Sites for Electrocatalysis. *Nat. Mater.* **2012**, *11*, 963–969.
17. Chen, Z.; Cummins, D.; Reinecke, B. N.; Clark, E.; Sunkara, M. K.; Jaramillo, T. F. Core–shell MoO₃–MoS₂ Nanowires for Hydrogen Evolution: A Functional Design for Electrocatalytic Materials. *Nano Lett.* **2011**, *11*, 4168–4175.
18. Merki, D.; Fierro, S.; Vrubel, H.; Hu, X. Amorphous Molybdenum Sulfide Films as Catalysts for Electrochemical Hydrogen Production in Water. *Chem. Sci.* **2011**, *2*, 1262–1267.
19. Benck, J. D.; Chen, Z.; Kuritzky, L. Y.; Forman, A. J.; Jaramillo, T. F. Amorphous Molybdenum Sulfide Catalysts for Electrochemical Hydrogen Production: Insights into the Origin of Their Catalytic Activity. *ACS Catal.* **2012**, *2*, 1916–1923.
20. Shin, S.; Jin, Z.; Kwon, D. H.; Bose, R.; Min, Y.-S. High Turnover Frequency of Hydrogen Evolution Reaction on Amorphous MoS₂ Thin Film Directly Grown by Atomic Layer Deposition. *Langmuir* **2015**, *31*, 1196–1202.
21. Kong, D.; Wang, H.; Cha, J. J.; Pasta, M.; Koski, K. J.; Yao, J.; Cui, Y. Synthesis of MoS₂ and MoSe₂ Films with Vertically Aligned Layers. *Nano Lett.* **2013**, *13*, 1341–1347.

- 1
2
3
4
5
6
7
8
9
10
11
12
13
14
15
16
17
18
19
20
21
22
23
24
25
26
27
28
29
30
31
32
33
34
35
36
37
38
39
40
41
42
43
44
45
46
47
48
49
50
51
52
53
54
55
56
57
58
59
60
22. Li, Y.; Wang, H.; Xie, L.; Liang, Y.; Hong, G.; Dai, H. MoS₂ Nanoparticles Grown on Graphene: An Advanced Catalyst for the Hydrogen Evolution Reaction. *J. Am. Chem. Soc.* **2011**, *133*, 7296–7299.
23. Lukowski, M. A.; Daniel, A. S.; Meng, F.; Forticaux, A.; Li, L.; Jin, S. Enhanced Hydrogen Evolution Catalysis from Chemically Exfoliated Metallic MoS₂ Nanosheets. *J. Am. Chem. Soc.* **2013**, *135*, 10274–10277.
24. Voiry, D.; Yamaguchi, H.; Li, J.; Silva, R.; Alves, D. C. B.; Fujita, T.; Chen, M.; Asefa, T.; Shenoy, V. B.; Eda, G.; *et al.* Enhanced Catalytic Activity in Strained Chemically Exfoliated WS₂ Nanosheets for Hydrogen Evolution. *Nat. Mater.* **2013**, *12*, 850–855.
25. Kang, Y.; Gong, Y.; Hu, Z.; Li, Z.; Qiu, Z.; Zhu, X.; Ajayan, P. M.; Fang, Z. Plasmonic Hot Electron Enhanced MoS₂ Photocatalysis in Hydrogen Evolution. *Nanoscale* **2015**, *7*, 4482–4488.
26. Benck, J. D.; Hellstern, T. R.; Kibsgaard, J.; Chakthranont, P.; Jaramillo, T. F. Catalyzing the Hydrogen Evolution Reaction (HER) with Molybdenum Sulfide Nanomaterials. *ACS Catal.* **2014**, *4*, 3957–3971.
27. Wang, T.; Liu, L.; Zhu, Z.; Papakonstantinou, P.; Hu, J.; Liu, H.; Li, M. Enhanced Electrocatalytic Activity for Hydrogen Evolution Reaction from Self-Assembled Monodispersed Molybdenum Sulfide Nanoparticles on an Au Electrode. *Energy Environ. Sci.* **2013**, *6*, 625–633.

- 1
2
3
4 28. Laursen, A. B.; Pedersen, T.; Malacrida, P.; Seger, B.; Hansen, O.; Vesborg, P. C. K.;
5
6 Chorkendorff, I. MoS₂—an Integrated Protective and Active Layer on N⁺p-Si for Solar
7
8 H₂ Evolution. *Phys. Chem. Chem. Phys.* **2013**, *15*, 20000–20004.
9
10
11 29. Benck, J. D.; Lee, S. C.; Fong, K. D.; Kibsgaard, J.; Sinclair, R.; Jaramillo, T. F.
12
13 Designing Active and Stable Silicon Photocathodes for Solar Hydrogen Production Using
14
15 Molybdenum Sulfide Nanomaterials. *Adv. Energy Mater.* **2014**, *4*, 1400739.
16
17
18 30. Jaramillo, T. F.; Jørgensen, K. P.; Bonde, J.; Nielsen, J. H.; Horch, S.; Chorkendorff, I.
19
20 Identification of Active Edge Sites for Electrochemical H₂ Evolution from MoS₂
21
22 Nanocatalysts. *Science* **2007**, *317*, 100–102.
23
24
25
26 31. Wang, H.; Zhang, Q.; Yao, H.; Liang, Z.; Lee, H.-W.; Hsu, P.-C.; Zheng, G.; Cui, Y.
27
28 High Electrochemical Selectivity of Edge versus Terrace Sites in Two-Dimensional
29
30 Layered MoS₂ Materials. *Nano Lett.* **2014**, *14*, 7138–7144.
31
32
33
34 32. Benson, J.; Li, M.; Wang, S.; Wang, P.; Papakonstantinou, P. Electrocatalytic Hydrogen
35
36 Evolution Reaction on Edges of a Few Layer Molybdenum Disulfide Nanodots. *ACS*
37
38 *Appl. Mater. Interfaces* **2015**, *7*, 14113–14122.
39
40
41
42 33. Tsai, C.; Chan, K.; Abild-Pedersen, F.; Nørskov, J. K. Active Edge Sites in MoSe₂ and
43
44 WSe₂ Catalysts for the Hydrogen Evolution Reaction: A Density Functional Study. *Phys.*
45
46 *Chem. Chem. Phys.* **2014**, *16*, 13156–13164.
47
48
49
50 34. Castellanos-Gomez, A.; Buscema, M.; Molenaar, R.; Singh, V.; Janssen, L.; Zant, H. S. J.
51
52 van der; Steele, G. A. Deterministic Transfer of Two-Dimensional Materials by All-Dry
53
54 Viscoelastic Stamping. *2D Mater.* **2014**, *1*, 011002.
55
56
57
58
59
60

- 1
2
3
4
5
6
7
8
9
10
11
12
13
14
15
16
17
18
19
20
21
22
23
24
25
26
27
28
29
30
31
32
33
34
35
36
37
38
39
40
41
42
43
44
45
46
47
48
49
50
51
52
53
54
55
56
57
58
59
60
35. Castellanos-Gomez, A.; Agraït, N.; Rubio-Bollinger, G. Optical Identification of Atomically Thin Dichalcogenide Crystals. *Appl. Phys. Lett.* **2010**, *96*, 213116.
36. Benameur, M. M.; Radisavljevic, B.; Héron, J. S.; Sahoo, S.; Berger, H.; Kis, A. Visibility of Dichalcogenide Nanolayers. *Nanotechnology* **2011**, *22*, 125706.
37. Lee, C.; Yan, H.; Brus, L. E.; Heinz, T. F.; Hone, J.; Ryu, S. Anomalous Lattice Vibrations of Single- and Few-Layer MoS₂. *ACS Nano* **2010**, *4*, 2695–2700.
38. Chakraborty, B.; Bera, A.; Muthu, D. V. S.; Bhowmick, S.; Waghmare, U. V.; Sood, A. K. Symmetry-Dependent Phonon Renormalization in Monolayer MoS₂ Transistor. *Phys. Rev. B* **2012**, *85*, 161403.
39. Miller, B.; Parzinger, E.; Vernickel, A.; Holleitner, A. W.; Wurstbauer, U. Photogating of Mono- and Few-Layer MoS₂. *Appl. Phys. Lett.* **2015**, *106*, 122103.
40. Tongay, S.; Zhou, J.; Ataca, C.; Liu, J.; Kang, J. S.; Matthews, T. S.; You, L.; Li, J.; Grossman, J. C.; Wu, J. Broad-Range Modulation of Light Emission in Two-Dimensional Semiconductors by Molecular Physisorption Gating. *Nano Lett.* **2013**, *13*, 2831–2836.
41. Nan, H.; Wang, Z.; Wang, W.; Liang, Z.; Lu, Y.; Chen, Q.; He, D.; Tan, P.; Miao, F.; Wang, X.; *et al.* Strong Photoluminescence Enhancement of MoS₂ through Defect Engineering and Oxygen Bonding. *ACS Nano* **2014**, *8*, 5738–5745.
42. Shi, H.; Yan, R.; Bertolazzi, S.; Brivio, J.; Gao, B.; Kis, A.; Jena, D.; Xing, H. G.; Huang, L. Exciton Dynamics in Suspended Monolayer and Few-Layer MoS₂ 2D Crystals. *ACS Nano* **2013**, *7*, 1072–1080.

- 1
2
3 43. Hill, H. M.; Rigosi, A. F.; Roquelet, C.; Chernikov, A.; Berkelbach, T. C.; Reichman, D.
4
5 R.; Hybertsen, M. S.; Brus, L. E.; Heinz, T. F. Observation of Excitonic Rydberg States
6
7 in Monolayer MoS₂ and WS₂ by Photoluminescence Excitation Spectroscopy. *Nano Lett.*
8
9 **2015**, *15*, 2992–2997.
10
11
12
13 44. Liu, H. J.; Jiao, L.; Xie, L.; Yang, F.; Chen, J. L.; Ho, W. K.; Gao, C. L.; Jia, J. F.; Cui,
14
15 X. D.; Xie, M. H. Molecular-Beam Epitaxy of Monolayer and Bilayer WSe₂: A Scanning
16
17 Tunneling Microscopy/spectroscopy Study and Deduction of Exciton Binding Energy.
18
19 *2D Mater.* **2015**, *2*, 034004.
20
21
22
23 45. Castellanos-Gomez, A.; Barkelid, M.; Goossens, A. M.; Calado, V. E.; van der Zant, H.
24
25 S. J.; Steele, G. A. Laser-Thinning of MoS₂: On Demand Generation of a Single-Layer
26
27 Semiconductor. *Nano Lett.* **2012**, *12*, 3187–3192.
28
29
30
31
32
33
34
35
36
37
38
39
40
41
42
43
44
45
46
47
48
49
50
51
52
53
54
55
56
57
58
59
60



TOC

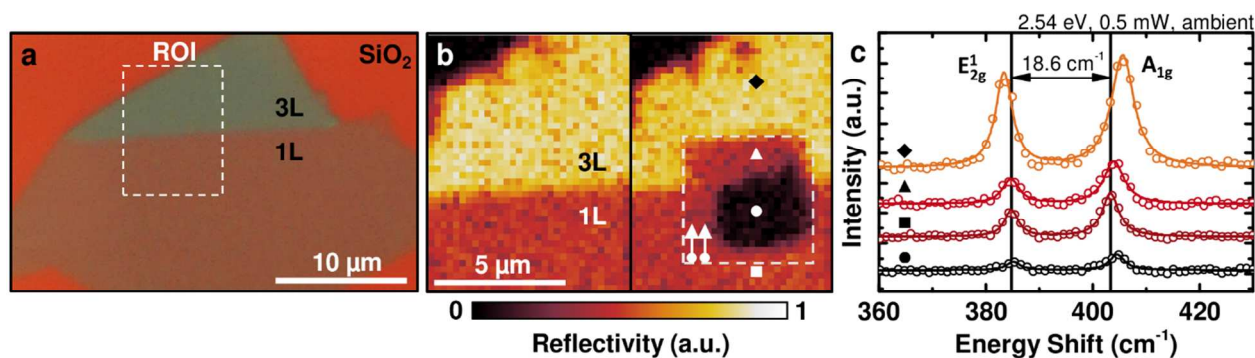


Figure 1. (a) Optical microscopy image (100x) of exfoliated single- (1L) and tri-layer (3L) MoS₂ on a Si/SiO₂ substrate. (b) Monochromatic reflectivity map of before (left) and after (right) a laser scan in the electrolyte of the ROI defined in (a). The arrows indicate scan direction. Step size 250 nm, dose 1 mW x 20 s at each spot. (c) Raman spectra of the spots marked in (b) of untreated, unaffected and photo-degraded regions.

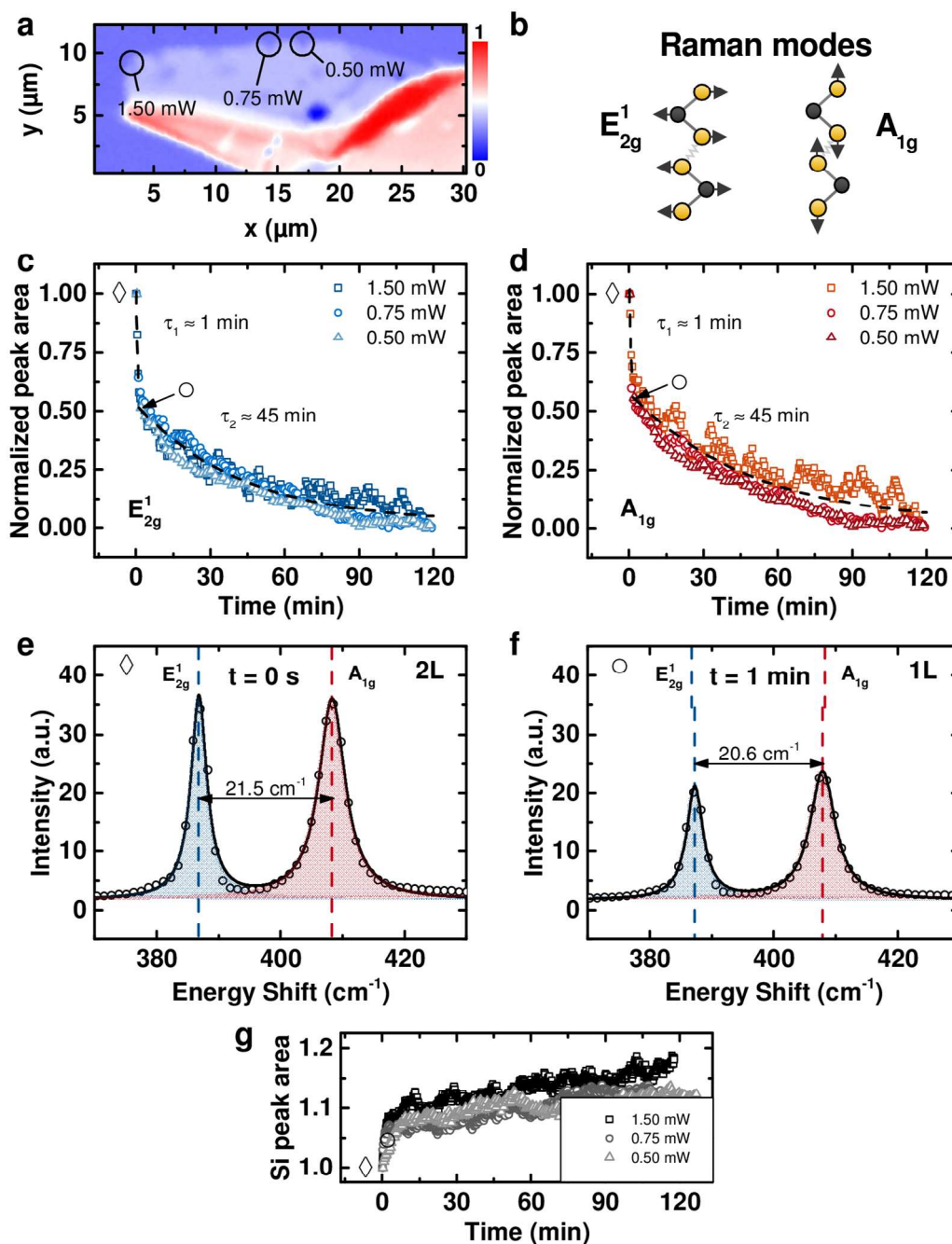


Figure 2. (a) Monochromatic reflectivity map of a MoS₂ bilayer sample after extensive photo-degradation measurements immersed in water (circles mark the corroded spots used for time-resolved measurements. More spots on the flake have been investigated). (b) Scheme of the direction of movement of Mo and S atoms for the two Raman active phonon modes E_{2g}¹ and A_{1g}, respectively. (c) and (d) Normalized Raman peak area intensity of the E_{2g}¹ (c) and A_{1g} (d) mode

1
2
3 of the spectra shown in (e) and (f) as a function of laser illumination time for the MoS₂ flake
4 immersed in DI water for various light intensities. The fits show two different decay rates for the
5 bilayer and the remaining monolayer-flake. (e) and (f) Raman spectra showing the E_{2g}¹ and A_{1g}
6 modes of an initial MoS₂ bilayer-flake (e) at the beginning of laser irradiation (◇) and (f) after
7 degradation from bi- to a monolayer after 1 min (○). (g) Raman peak area intensity of the silicon
8 TO-phonon mode that depicts the complementary increase of the Raman signal originating from
9 the substrate.
10
11
12
13
14
15
16
17
18
19
20
21
22
23
24
25
26
27
28
29
30
31
32
33
34
35
36
37
38
39
40
41
42
43
44
45
46
47
48
49
50
51
52
53
54
55
56
57
58
59
60

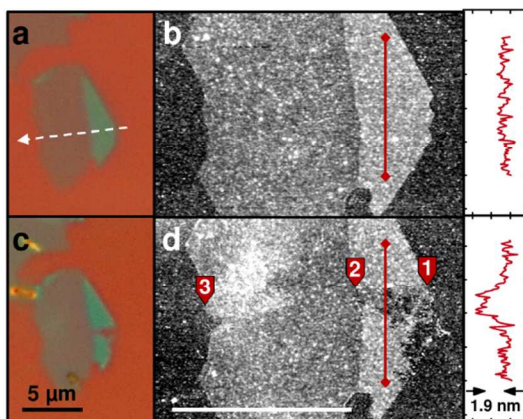


Figure 3. (a, c) Optical microscopy (100x) and (b, d) AFM image of exfoliated single- and trilayer flake on a Si/SiO₂ substrate before (top) and after (bottom) laser linescan immersed in electrolyte. The dashed arrow indicates the scan direction. The steps from substrate to trilayer (1), from trilayer to monolayer (2) and from monolayer to substrate (3) are highlighted with labels. Photo-degradation takes predominantly place on edge sites. The corresponding AFM height-profiles at the trilayer regions are depicted on the right (red lines). Scale bars 5 μm.

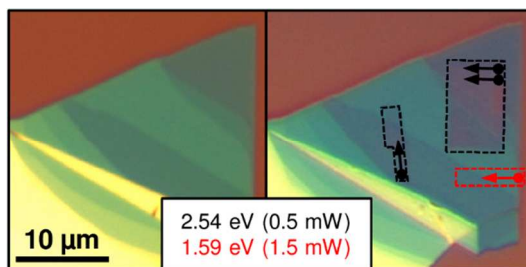


Figure 4. Optical microscopy image of a multi-layer MoS₂ flake before (left) and after (right) area illumination scans with a laser energy below (1.59 eV) and above (2.54 eV) the direct band gap, respectively. The MoS₂ flake is unaffected for exposure to light with energy smaller than the band-gap (red marked area). In case of illumination with energy larger than the band gap, corrosion of the MoS₂ flake is clearly visible (black marked areas). Scan parameters: step size 250 nm, illumination at each spot: 21 s.

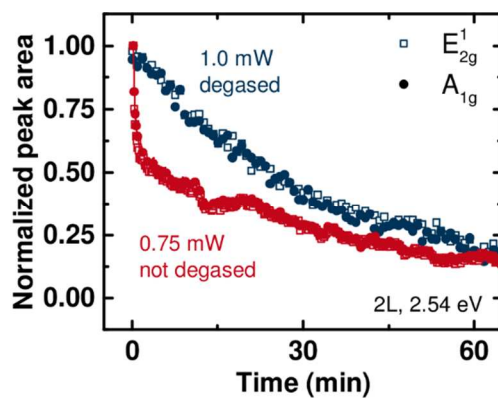


Figure 5. Normalized Raman peak area of the E_{2g}^1 and A_{1g} mode as a function of laser illumination time on the edge site of a bilayer-flake. The upper curve (blue) corresponds to a flake immersed in water with reduced oxygen concentration in the electrolyte, the lower curve (red) to water with a natural amount of dissolved oxygen.